On the use of thin structures to control the far-field properties of an acoustic devices

Esubalewe Lakie Yedeg

Department of Computing Science,
Umeå University, SE–901 87 Umeå, Sweden

Abstract

This work presents a sensitivity analysis for topology optimization of thin structures inside an acoustic horn in order to improve its far-field directivity properties. The objective function gradient is computed using an adjoint-based method, a well-known approach in the design optimization community due to its ability to compute the design sensitivities when there is a large number of design variables. The accuracy of the computed gradient is verified numerically against a first order finite difference approximation. The report also covers the matrix representations of the far-field pattern evaluation and the variational problem with an interface condition to model the thin structures.

1 Introduction

Topology optimization is a strategy to determine the layout of material in devices such that some measure of performance is maximized. For topology optimization, the shape as well as the connectedness of the individual parts of a device are subject to optimization. The most common way of performing such optimization is through the *material distribution* approach [1]. In the material distribution, a design region is divided into a large number of small elements ("pixels" in 2D and "voxels" in 3D) and the optimization algorithm decides about the material composition of each element. Relaxation, penalization, and *design filters* are techniques that are typically used together with the material distribution approach [1]. Design filters replace the design variable at a particular element by an average of the design variables in a predefined filter radius. This approach has the tendency to produce designs with extended volumes of material or void and thus to filter out thin structures.

For acoustic devices, it is possible to get significant effects on the acoustic wave propagation without adding extended volumes of materials by an appropriate placement of thin structures with suitable material properties. The material distribution approach applied to the design of acoustic devices has consequently a tendency to create thin [2] and scattered [3] structures. It therefore appears natural, for design of acoustic

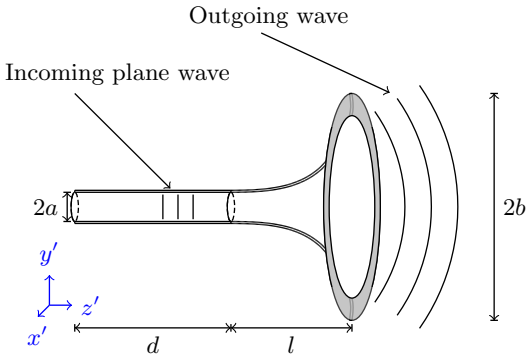

Figure 1: The horn to be optimized connected with a cylindrical waveguide.

devices, to consider methods that can distribute thin materials instead of the standard "volumetric" material distribution to topology optimization technique [1].

Acoustic properties of thin materials can be modeled by an *acoustic transmission impedance* Z, defined as the ratio of effective pressure jump over the surface to the effective normal acoustic velocity through the surface [4, 5]. The limit cases $|Z| = 0$ and $|Z| \to \infty$ model a vanishing and a sound-hard surface, respectively. As discussed in § 4 below, the standard finite element formulation has a term proportional to the inverse of the transmission impedance and can not be used with a vanishing surface. Recently, we introduced a new finite element method [6], which seamlessly handles both vanishing and non-vanishing surface impedance.

We aim to demonstrate a technique for layout optimization of thin structures in the context of an acoustic horn, where thin structures will be placed inside the horn in order to improve the far-field directivity properties. The optimization will be carried out using a gradient-based algorithm. We thus need the derivatives of both the objective and constraint functions with respect to the design variables.

This report contains a detailed account on some technical details in preparation for the optimization study. In particular, we present matrix representation for evaluations of the far-field pattern and the sensitivity analysis of the problem. The sensitivity analysis is performed by using the adjoint equation method [7, § 6] and we verify the accuracy of the computed objective function gradient with the finite difference approximations.

2 Governing Equation

We consider the cylindrically symmetric horn conceptually illustrated in Figure 1. The horn is connected with a cylindrical feeding waveguide. For the purpose of numerical computations, we truncate the exterior domain of wave propagation into a domain Ω bounded by an artificial boundary Γ_{out}, as shown in Figure 2. Moreover, we ssume that

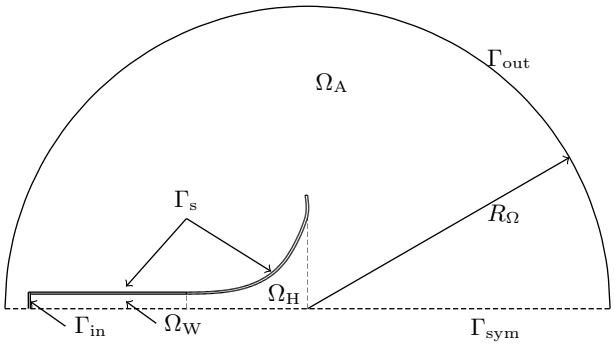

Figure 2: The computational domain of the optimization problem.

Ω is the union of three disjoint, open, and connected subdomains Ω_{W}, Ω_{H}, and Ω_{A}, that is, $\overline{\Omega} = \overline{\Omega}_{\text{W}} \cup \overline{\Omega}_{\text{H}} \cup \overline{\Omega}_{\text{A}}$. Here, Ω_{W} is the region between symmetry line and the waveguide boundary, Ω_{H} is the region between the horn and symmetry line, and Ω_{A}, the region outside the horn and the waveguide regions and bounded by an artificial boundary. The boundaries of the computational domain are denoted by Γ_{in}, the left boundary of the truncated waveguide; Γ_{out}, a fictitious far-field boundary where the exterior domain is truncated; Γ_{sym}, an axial symmetry line; and Γ_{s}, the boundary composed of the boundaries of the waveguide and horn.

We consider single-frequency time-harmonic solutions of the linear wave equation and thus assume that the time varying pressure field is separated as $P(\psi, t) = \Re(p(\psi)\mathrm{e}^{\mathrm{i}\omega t})$, where $\Re$ is the real part, p is a complex amplitude function, ω is the angular frequency, $\psi = (r, z)$, and $\mathrm{i}^2 = -1$. We consider the following boundary value problem for Helmholtz equation,

$$\nabla \cdot (r\nabla p) + \kappa^2 r p = 0 \qquad \text{in } \Omega_0, \tag{1a}$$

$$\left(\mathrm{i}\kappa + \frac{1}{R_\Omega}\right) p + \frac{\partial p}{\partial n} = 0 \qquad \text{on } \Gamma_{\text{out}}, \tag{1b}$$

$$\mathrm{i}\kappa p + \frac{\partial p}{\partial n} = 2\mathrm{i}\kappa A \qquad \text{on } \Gamma_{\text{in}}, \tag{1c}$$

$$\frac{\partial p}{\partial n} = 0 \qquad \text{on } \Gamma_{\text{s}} \cup \Gamma_{\text{sym}}, \tag{1d}$$

where $\nabla = (\partial/\partial r, \partial/\partial z)$, r is the radial coordinate, and κ/c is the wave number, in which c is the speed of sound. Condition (1b) is a first order Engquist–Majda absorbing boundary condition [8, 9], which approximates the Sommerfeld radiation condition, that is, the requirement that all waves are outgoing in the far-field. Condition (1c) imposes an incoming plane wave of amplitude A at Γ_{in} while ensuring that out-going plane waves are absorbed.

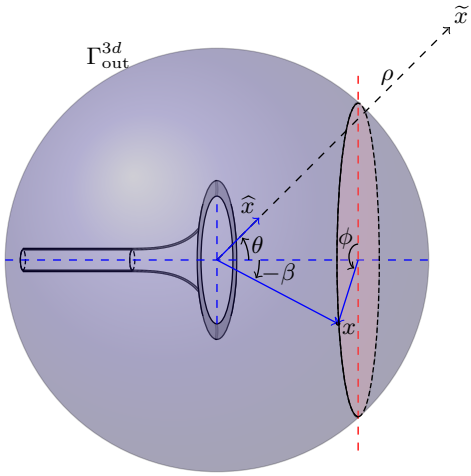

Figure 3: A sphere Γ^{3d}_{out} of radius R_Ω enclosing all sound sources and notations used for far-field calculations.

3 Far-field directivity pattern

An important property of an acoustic horn is its far-field directivity characterstics, which describes the angular dependancy of the acoustic intensity. Let $\widehat{p}$ be a solution of the exterior Helmholtz equation (1a) respecting the Sommerfeld radiation condition, $\widehat{x}(\theta)$ be a point on the unit sphere at an angle θ with respect to the symmetry axis, and $\rho > 0$ be a distance of point $\widetilde{x} = \rho\widehat{x}(\theta)$ from the device as shown in Figure 3. Here, we assume that the horn is the only source of sound and that it is enclosed inside a sphere Γ^{3d}_{out}. The Sommerfeld radiation condition yields the following asymptotic behaviour as $\rho \to \infty$ [10, 11]

$$\widehat{p}(\widetilde{x}) = \frac{e^{-\mathrm{i}\kappa\rho}}{\rho}\left\{p_\infty(\theta) + O(\frac{1}{\rho})\right\}. \tag{2}$$

Here the function $p_\infty(\theta)$, which characterizes the angular dependance of $\widehat{p}$ in the far-field, is called the far-field pattern.

Classical methods from scattering theory [10, 11], yields the following expression for the far-field pattern at an angle θ with respect to the symmetry axis:

$$p_\infty(\theta) = \frac{1}{4\pi}\int_{\Gamma^{3d}_{\text{out}}} e^{\mathrm{i}\kappa\widehat{x}\cdot x}\left(\mathrm{i}\kappa\widehat{p}\widehat{x}\cdot n - \frac{\partial\widehat{p}}{\partial n}\right), \tag{3}$$

where n is an outward directed unit-normal vector of Γ_{out}. Due to the symmetry assumption, the boundary Γ^{3d}_{out} can be generated by rotating Γ_{out} around the symmetry line Γ_{sym}. By substituting the solution p of the truncated problem satisfying boundary

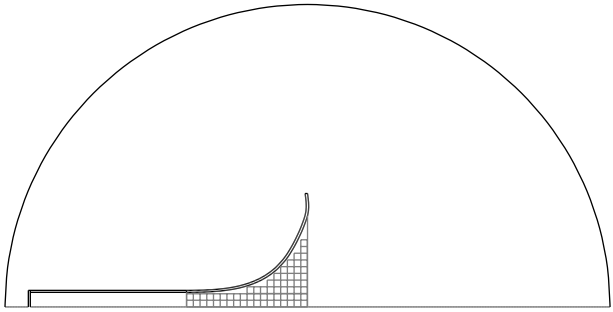

Figure 4: A design grid consisting of squares inside the design region Ω_{H}

condition (1b), we get

$$p_\infty(\theta) = \frac{1}{4\pi} \int_{\Gamma^{3d}_{\mathrm{out}}} e^{\mathrm{i}\kappa\widehat{x}\cdot x} \left(\frac{1}{R_\Omega} + \mathrm{i}\kappa + \mathrm{i}\kappa\widehat{x} \cdot n \right) p. \tag{4}$$

4 Variational problem

The aim of the optimization is to improve the performance of the given horn by distributing thin sheets of sound-hard material along a grid inside the *design region*, Ω_{H}. We therefore introduce a design grid consisting of squares as depicted in Figure 4. These squares partition the computational domain into several small subdomains and introduce multiple interface boundaries between the subdomains. We denote the union of all interface boundaries by Γ_{I} and define $\Omega_0 = \Omega \setminus \Gamma_{\mathrm{I}}$.

The acoustic properties of the interface is modeled using a transmission impedance. Denote the normalized transmission impedance by $\zeta = Z/(\rho c)$, where ρ is the air density. Then, by assuming the normal flux of the acoustic pressure is continuous over the interface, we have (see Section 2.1 of Yedeg et al. [6] for a derivation)

$$\frac{\mathrm{i}k}{\zeta} [\![p]\!] + \left\{ \frac{\partial p}{\partial n} \right\} = 0 \qquad \text{on } \Gamma_{\mathrm{I}}, \tag{5}$$

where for two neighbouring subdomains Ω_i and Ω_j, having a common interface boundary, the pressure jump and average acoustic flux over the interface are defined by

$$[\![p]\!] = \boldsymbol{n} \cdot (\boldsymbol{n}_i p_i + \boldsymbol{n}_j p_j), \tag{6}$$

$$\left\{ \frac{\partial p}{\partial n} \right\} = \frac{1}{2} \left(\frac{\partial p_i}{\partial n} + \frac{\partial p_j}{\partial n} \right). \tag{7}$$

Here p_i and p_j are the limits of acoustic pressure when approaching the interface from the interior of Ω_i and Ω_j, respectively and $\boldsymbol{n}_i$ and $\boldsymbol{n}_j = -\boldsymbol{n}_i$ are the two outward-directed unit normal vectors on each side of the interface.

Multiplying Helmholtz equation (1a) by a test function and applying integration by parts, using boundary conditions (1b)–(1d) and (5), we obtain the following variational problem.

$$\begin{aligned} &\text{Find } p \in H^1(\Omega_0) \text{ such that} \\ &\quad a(p,q) = \ell(q) \ \ \forall q \in H^1(\Omega_0), \end{aligned} \tag{8}$$

where the linear functional ℓ is defined by

$$\ell(q) = 2\mathrm{i}\kappa A \int_{\Gamma_{\text{in}}} rq \tag{9}$$

and the bilinear form a is given by

$$a(p,q) = \int_{\Omega_0} r\nabla p \cdot \nabla q - \kappa^2 \int_{\Omega_0} rpq + \mathrm{i}\kappa \int_{\Gamma_{\text{in}}\cup\Gamma_{\text{out}}} rpq + \frac{1}{R_\Omega} \int_{\Gamma_{\text{out}}} rpq + \mathrm{i}\kappa \int_{\Gamma_{\text{I}}} \frac{r}{\zeta} [\![p]\!][\![q]\!]. \tag{10}$$

Note that, since Ω_0 is a disconnected space due to the presence of interface Γ_{I}, the space $H^1(\Omega_0)$ contains functions that are discontinuous over Γ_{I}.

Remark 1. Throughout the article, we do not explicitly specify the measure symbol (such as $\mathrm{d}\Omega$ or $\mathrm{d}\Gamma$, for instance) in the integrals, since the type measure will be clear from the domain of integration.

We characterize the structure of Γ_{I} by using a material indicator function $\alpha : \Gamma_{\text{I}} \to \{0,1\}$ defined such that $\alpha(x) = 0$ if x is occupied by material and $\alpha(x) = 1$ if x is occupied by air. Then, we define the impedance function as $\zeta = \zeta(\alpha)$ such that $\zeta = 0$ when $\alpha = 1$ for a vanishing interface and when $\alpha = 0$, ζ attains its allowed maximum value, which approximates the impedance of a sound-hard material.

5 Optimization objective function

We aim for an even distribution of sound pressure in some listening area in front of the device. The main objective of the optimization will be to reduce the variation of far-field intensities between different angles. To minimize the difference in magnitude of the far-field intensities at two given angles θ_1 and θ_2, for given frequency f and design α, we consider the objective function

$$J(\alpha; f, \theta_1, \theta_2) = \frac{1}{2} \log_{10} \left(\frac{|p_\infty(\theta_1)|^2}{|p_\infty(\theta_2)|^2} \right), \tag{11}$$

where p_∞ is as defined in expression (4).

In order to enable the use of a gradient-based optimization algorithm, we relax the design variable to attain any value in the range $[0,1]$ and define the set of feasible designs by

$$\mathcal{U} = \Big\{ \alpha \in L^\infty(\Gamma_{\text{I}}) : 0 \le \alpha \le 1 \text{ a.e. in } \Gamma_{\text{I}} \Big\}. \tag{12}$$

Then, the optimization problem is formulated as follows

$$\min_{\alpha\in\mathcal{U}} J(\alpha; f, \theta_1, \theta_2), \tag{13}$$

where for $k = 2\pi f/c$ and $\zeta = \zeta(\alpha)$, $p \in H^1(\Omega_0)$ solves

$$a(p, q) = \ell(q) \ \ \forall q \in H^1(\Omega_0). \tag{14}$$

6 Discrete problem

Provided that $|\zeta|$ is bounded away from zero, a standard finite element method can directly be used to discretize variational form (8). However, this discretization leads to an ill-conditioned system matrix as $\zeta \to 0$ on a set of positive measure on Γ_{I}. Morover, if $\zeta = 0$ on a portion of Γ_{I}, the standard finite element discretization can not be used because the bilinear form a defined in expression (10) will be undefined. To handle both vanishing and non-vanishing interface conditions seamlessly, we use a new finite element method [6] based on a variant of Nitsche's method [12]

We introduce families of non-degenerate triangulations $\left\{\mathcal{T}_i^h\right\}_{h>0}$ of the subdomains Ω_i, $i = 1, \ldots, n_\Omega$, where n_Ω is the number of subdomains that constitute Ω. Define $h = \max_{K\in\bigcup_i^{n_\Omega}\mathcal{T}_i^h} h_K$, where h_K is the diameter of element K. Let V_i^h be the space of all complex-valued, continuous functions that are bi-quadratic polynomials on each element in Ω_i and extended by zero into $\Omega \setminus \Omega_i$. We define the finite element space by $V_h = \sum_i V_i^h$.

The solution of the acoustic problem $p \in H^1(\Omega_0)$ is approximated in the space V_h and denoted by p_h. Let $\alpha_h : \Gamma_{\mathrm{I}} \to [0, 1]$ be an edgewise constant function that approximates the material indicator function α. Similarly, the impedance function ζ is approximated by edgewise function $\zeta_h = \zeta(\alpha_h)$.

6.1 Discrete state equation

The discrete version of variational problem (8), based on a Nitsche-type formulation, is defined as follows.

$$\begin{aligned} &\text{Find } p_h \in V_h \text{ such that} \\ &\quad a_\lambda(p_h, q_h) = \ell(q_h) \ \ \forall q_h \in V_h, \end{aligned} \tag{15}$$

where

$$\begin{aligned} a_\lambda(p_h, q_h) = &\int_{\Omega_0} r\nabla p_h \cdot \nabla q_h - \kappa^2 \int_{\Omega_0} r p_h q_h + \mathrm{i}\kappa \int_{\Gamma_{\mathrm{in}}\cup\Gamma_{\mathrm{out}}} r p_h q_h + \int_{\Gamma_{\mathrm{I}}} r\lambda [\![p_h]\!][\![q_h]\!] \\ &- \int_{\Gamma_{\mathrm{I}}} r c_1 \Big([\![q_h]\!] \left\{ \frac{\partial p_h}{\partial n} \right\} + [\![p_h]\!] \left\{ \frac{\partial q_h}{\partial n} \right\} \Big) - \int_{\Gamma_{\mathrm{I}}} r c_2 \left\{ \frac{\partial p_h}{\partial n} \right\} \left\{ \frac{\partial q_h}{\partial n} \right\}, \end{aligned} \tag{16}$$

in which

$$c_1 = 1 - \lambda \frac{\zeta_h}{\mathrm{i}\kappa},$$
$$c_2 = \frac{\zeta_h}{\mathrm{i}\kappa}\big(1 - \lambda \frac{\zeta_h}{\mathrm{i}\kappa}\big), \tag{17}$$

and the function $\lambda \in L^\infty(\Gamma_\mathrm{I})$ is defined by

$$\lambda = \left(\frac{h}{\gamma} + \frac{\zeta_h}{\mathrm{i}\kappa}\right)^{-1}, \tag{18}$$

for a sufficiently large parameter $\gamma > 0$. Here it will hold that $\operatorname{Im} \zeta_h \geq 0$, which means that λ will be a nonzero and bounded function. For an analysis of problem (15) see Yedeg et al. [6].

6.2 Discrete objective functions

For a single frequency f, the discrete form of the far-field pattern in expression (4) is obtained by replacing p with p_h

$$p_{h,\infty}(\theta) = \frac{1}{4\pi} \int_{\Gamma^{3d}_{\mathrm{out}}} e^{\mathrm{i}\kappa \widehat{x} \cdot x} \left(\frac{1}{R_\Omega} + \mathrm{i}\kappa + \mathrm{i}\kappa \widehat{x} \cdot n\right) p_h. \tag{19}$$

Here $p_h(\alpha_h, f)$ is the solution of the discrete state equation (15) with impedance $\zeta_h = \zeta(\alpha_h)$ and wave number $\kappa = 2\pi f/c$. Then, the discrete form of objective function (11), to minimize the difference in magnitude of the far-field intensity between two angles θ_1 and θ_2 is

$$J_h(\alpha_h; f, \theta_1, \theta_2) = \frac{1}{2} \log_{10} \left(\frac{|p_{h,\infty}(\theta_1)|^2}{|p_{h,\infty}(\theta_2)|^2}\right). \tag{20}$$

7 Matrix representation of the state equation and the far-field pattern

The solutions of the discrete bilinear problem (15) can be written as

$$p_h = \sum_{i=1}^{N_n} p_i \psi_i, \tag{21}$$

where $\psi_i \in V_h$ is a standard nodal basis function. Note that the nodes on the interface are doubled, since the functions should support jump discontinuities over the interface. Define $\mathbf{p} = (p_1, p_2, \ldots, p_{N_n})^{\mathrm{T}}$ and $\mathbf{e} = (1, 1, \ldots, 1)^{\mathrm{T}}$ with size $N_n \times 1$. Then the matrix form of the discrete state equation (15) is

$$\Big(\mathbf{K} - \kappa^2 \mathbf{M} + \mathrm{i}\kappa \mathbf{M}^{\mathrm{in\_out}} + \frac{1}{R_\Omega} \mathbf{M}^{\mathrm{out}} - (\mathbf{N}^{\mathrm{I}_1} + [\mathbf{N}^{\mathrm{I}_1}]^{\mathrm{T}}) - \mathbf{N}^{\mathrm{I}_2} + \mathbf{M}^{\mathrm{I}}\Big)\mathbf{p} = 2\mathrm{i}\kappa \mathbf{M}^{\mathrm{in}} \mathbf{e}. \tag{22}$$

In equation (22), the elements of stiffness and mass matrices $\mathbf{K}$ and $\mathbf{M}$ are given by

$$\begin{cases}\mathbf{K}_{ij} = \int_{\Omega_0} r\nabla\psi_i \cdot \nabla\psi_j, \\ \mathbf{M}_{ij} = \int_{\Omega_0} r\psi_i\psi_j, \end{cases} \qquad i,j \in \{1,2,\ldots,N_n\}, \tag{23}$$

respectively. The components of the boundary matrices $\mathbf{M}^{\text{in}}$, $\mathbf{M}^{\text{out}}$, and $\mathbf{M}^{\text{in\_out}}$ are

$$\begin{cases}\mathbf{M}^{\text{in}}_{ij} = \int_{\Gamma_{\text{in}}} r\psi_i\psi_j, \\ \mathbf{M}^{\text{out}}_{ij} = \int_{\Gamma_{\text{out}}} r\psi_i\psi_j, \\ \mathbf{M}^{\text{in\_out}}_{ij} = \int_{\Gamma_{\text{in}}\cup\Gamma_{\text{out}}} r\psi_i\psi_j, \end{cases} \qquad i,j \in \{1,2,\ldots,N_n\}, \tag{24}$$

respectively. To define the matrices from the interface boundary integrals, let i and j be two nodes on Γ_{I} and corresponding nodal basis function ψ_i and ψ_j. Denote the supports of ψ_i and ψ_j by $S_i = \operatorname{supp}\psi_i$ and $S_j = \operatorname{supp}\psi_j$, respectively. Assume that $S_i \cap S_j \neq \emptyset$. Then there are two neighbouring subdomains Ω_l and Ω_m, with a common interface boundary such that either $S_i, S_j \subset \Omega_l$ or $S_i, S_j \subset \Omega_m$ or $S_i \subset \Omega_l$ and$S_j \subset \Omega_m$. Now we fix the orientation by choosing $\mathbf{n} = \mathbf{n}_l = -\mathbf{n}_m$. Define the matrices $\mathbf{C}^{LL}$, $\mathbf{C}^{LR}$, and $\mathbf{C}^{RR}$ with the nonzero components

$$\begin{cases}\mathbf{C}^{LL}_{ij} = \int_{\Gamma_{\text{I}}} r\lambda\psi_i\psi_j & \text{if } S_i, S_j \subset \Omega_l, \\ \mathbf{C}^{LR}_{ij} = \int_{\Gamma_{\text{I}}} r\lambda\psi_i\psi_j & \text{if } S_i \subset \Omega_l \text{ and } S_j \subset \Omega_m, \\ \mathbf{C}^{RR}_{ij} = \int_{\Gamma_{\text{I}}} r\lambda\psi_i\psi_j & \text{if } S_i, S_j \subset \Omega_m, \end{cases} \tag{25}$$

then we have $\mathbf{M}^{\text{I}} = \mathbf{C}^{LL} - \mathbf{C}^{LR} - [\mathbf{C}^{LR}]^{\text{T}} + \mathbf{C}^{RR}$. Similarly, we have $\mathbf{N}^{\text{I}_1} = 0.5(\mathbf{D}^{LL} + \mathbf{D}^{LR} - \mathbf{D}^{RL} - \mathbf{D}^{RR})$, where the sub-matrices have the nonzero components

$$\begin{cases}\mathbf{D}^{LL}_{ij} = \int_{\Gamma_{\text{I}}} rc_1\psi_i\frac{\partial\psi_j}{\partial n} & \text{if } S_i, S_j \subset \Omega_l, \\ \left.\begin{aligned}\mathbf{D}^{LR}_{ij} &= \int_{\Gamma_{\text{I}}} rc_1\psi_i\frac{\partial\psi_j}{\partial n} \\ \mathbf{D}^{RL}_{ij} &= \int_{\Gamma_{\text{I}}} rc_1\psi_j\frac{\partial\psi_i}{\partial n}\end{aligned}\right\} & \text{if } S_i \subset \Omega_l \text{ and } S_j \subset \Omega_m, \\ \mathbf{D}^{RR}_{ij} = \int_{\Gamma_{\text{I}}} rc_1\psi_i\frac{\partial\psi_j}{\partial n} & \text{if } S_i, S_j \subset \Omega_m, \end{cases} \tag{26}$$

and $\mathbf{N}^{\text{I}_2} = 0.25(\mathbf{E}^{LL} + \mathbf{E}^{LR} + [\mathbf{E}^{LR}]^{\text{T}} + \mathbf{E}^{RR})$, where the sub-matrices have the nonzero components

$$\begin{cases}\mathbf{E}^{LL}_{ij} = \int_{\Gamma_{\text{I}}} rc_2\frac{\partial\psi_i}{\partial n}\frac{\partial\psi_j}{\partial n} & \text{if } S_i, S_j \subset \Omega_l, \\ \mathbf{E}^{LR}_{ij} = \int_{\Gamma_{\text{I}}} rc_2\frac{\partial\psi_i}{\partial n}\frac{\partial\psi_j}{\partial n} & \text{if } S_i \subset \Omega_l \text{ and} S_j \subset \Omega_m, \\ \mathbf{E}^{RR}_{ij} = \int_{\Gamma_{\text{I}}} rc_2\frac{\partial\psi_i}{\partial n}\frac{\partial\psi_j}{\partial n} & \text{if } S_i, S_j \subset \Omega_m. \end{cases} \tag{27}$$

To formulate a matrix representation of the far-field pattern, let us rewrite expression (19) as fillows

$$p_{h,\infty}(\theta) = \int_{\Gamma_{\text{out}}} \left[\int_0^{2\pi} \frac{1}{4\pi} e^{\text{i}\kappa\widehat{x}\cdot x}\left(\frac{1}{R_\Omega} + \text{i}\kappa + \text{i}\kappa\widehat{x}\cdot n\right)\mathrm{d}\phi\right] p_h \,\mathrm{d}\Gamma = \int_{\Gamma_{\text{out}}} f_\theta p_h \,\mathrm{d}\Gamma, \tag{28}$$

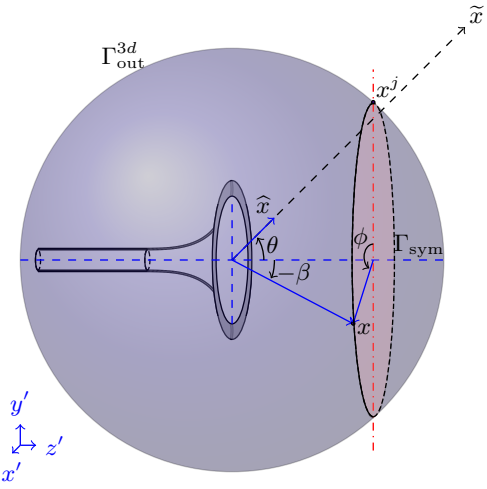

Figure 5: Geometric notations used for the far-field calculations. Here x^j is a node on Γ_{out} lying in the $z'y'$ plane (Γ_{out} is used to generate Γ_{out}^{3d} by rotation through Γ_{sym}), β is the angle between node x^j and the symmetry line, $\widehat{x}$ is a unit vector in the direction of θ lying in the $z'y'$ plane, x is a point on the sphere obtained by rotating x^j through an angle ϕ with respect to the $z'y'$ plane.

where

$$f_\theta = \int_0^{2\pi} \frac{1}{4\pi} e^{\mathrm{i}\kappa\widehat{x}\cdot x} \left(\frac{1}{R_\Omega} + \mathrm{i}\kappa + \mathrm{i}\kappa\widehat{x}\cdot n \right) \mathrm{d}\phi. \tag{29}$$

Now by interpolating function f_θ in space V_h, the far-field pattern defined in expression (19) can be written in matrix form as

$$p_{h,\infty}(\theta) = \mathbf{f}_\theta^{\mathrm{T}} \mathbf{M}^{\text{out}} \mathbf{p}, \tag{30}$$

where $\mathbf{M}^{\text{out}}$ is a matrix defined in expression (24), and the nonzero elements of vector $\mathbf{f}_\theta$ is calculated as follows. Let x^j be a node on Γ_{out} and let $\beta \in [0, \pi]$ be the angle between node x^j and the symmetry line Γ_{sym} so that $x^j = R_\Omega\big(0, \cos\beta, \sin\beta\big)$. Let $x = R_\Omega\big(\sin\beta\sin\phi, \cos\beta, \sin\beta\sin\phi\big)$ be a point in Γ_{out}^{3d} obtained by rotating x^j around Γ_{sym} by an angle ϕ. Here $\phi \in [0, 2\pi]$ is the angle between point x and the vertical line through node x^j (dash-dotted line in Figure 5). Note that the angle between x and the symmetry line Γ_{sym} is β. Also note that the unit normal vector on Γ_{out}^{3d} at a point x is $n = x/R_\Omega$. Using the symmetry assumption, we choose the point in the unit sphere $\widehat{x}(\theta) = \big(0, \cos\theta, \sin\theta\big)$. Then we have

$$\begin{aligned} \widehat{x}\cdot x &= R_\Omega\big(\cos\beta\cos(\theta) + \sin\beta\sin\theta\cos\phi\big), \\ \widehat{x}\cdot n &= \cos\beta\cos(\theta) + \sin\beta\sin\theta\cos\phi. \end{aligned} \tag{31}$$

The j^{th} nonzero component of $\mathbf{f}_\theta$, using expression (31), is given by

$$f_\theta^j = \frac{1}{4\pi}\int_0^{2\pi} e^{\mathrm{i}\kappa R_\Omega\left(a+b\cos\phi\right)}\left(\frac{1}{R_\Omega}+\mathrm{i}\kappa+\mathrm{i}\kappa\big(a+b\cos\phi\big)\right)\mathrm{d}\phi, \tag{32}$$

where $a=\cos\beta\cos(\theta)$ and $b=\sin\beta\sin\theta$. Using Euler's formula ($e^{\mathrm{i}\varphi}=\cos\varphi+\mathrm{i}\sin\varphi$ for any real number φ) and $\cos\phi = 0.5(e^{\mathrm{i}\phi}+e^{-\mathrm{i}\phi})$, we can rewrite expression (32) as

$$\begin{aligned} f_\theta^j =& \frac{e^{\mathrm{i}\kappa R_\Omega a}}{4\pi}\Bigg[\Big(\frac{1}{R_\Omega}+\mathrm{i}\kappa+\mathrm{i}\kappa a\Big)\int_0^{2\pi} e^{\mathrm{i}\kappa R_\Omega b\cos\phi}\,\mathrm{d}\phi + \\ & \frac{\mathrm{i}\kappa b}{2}\Big(\int_0^{2\pi} e^{\mathrm{i}(\phi+\kappa R_\Omega b\cos\phi)}\,\mathrm{d}\phi+\int_0^{2\pi} e^{\mathrm{i}(-\phi+\kappa R_\Omega b\cos\phi)}\,\mathrm{d}\phi\Big)\Bigg]. \end{aligned} \tag{33}$$

Expression (33) can be rewritten using Bessel function of the first kind of order $-1,0,1$ and argument $\kappa R_\Omega b$ [13]. The integrals in expression (33) are approximated by the trapezoidal rule.

8 Sensitivity Analysis

For an arbitrary interface boundary mesh element E_i in Γ_{I}, let a_i denote the value on E_i of the piecewise constant functions α_h. Let N_Γ be the number of interface boundary elements in Γ_{I} and define the vector representation of α_h by $\mathbf{a}=(a_1,\ldots,a_{N_\Gamma})^T$. For a gradient-based optimization method, we need the derivative of the objective function with respect to the design variable $\mathbf{a}$. But the objective function J_h depend on $\mathbf{a}$ only implicitly through state equation (15). We use the adjoint-based method [7, § 6] to compute the gradient of the objective function.

We rewrite the mean square pressure in the far-field at an angle θ as

$$I_h(\theta) = |p_{h,\infty}(\theta)|^2 = g_1^2+g_2^2, \tag{34}$$

where g_1 and g_2 are the real and imaginary part of $p_{h,\infty}(\theta)$, respectively. Then, the gradient of the mean square pressure with respect to $\mathbf{a}$, using the chain rule, is given by

$$\nabla_{\mathbf{a}} I_h(\theta) = 2g_1\nabla_{\mathbf{a}}g_1 + 2g_2\nabla_{\mathbf{a}}g_2. \tag{35}$$

Next, we derive the adjoint-based computation of the gradients of g_1 and g_2.

Let $\delta\alpha_h$ be an arbitrary variation of the design variable α_h. Then under a variation $\delta\alpha_h$, the first variation of the functions g_1 and g_2 can be expressed as

$$\begin{aligned} \delta g_1 &= \delta\Re\{p_{h,\infty}(\theta)\} = \Re\{\delta p_{h,\infty}(\theta)\}, \\ \delta g_2 &= \delta\Im\{p_{h,\infty}(\theta)\} = \Im\{\delta p_{h,\infty}(\theta)\}, \end{aligned} \tag{36}$$

respectively, where $\Im$ is the imaginary part and

$$\delta p_{h,\infty}(\theta) = \frac{1}{4\pi}\int_{\Gamma_{\text{out}}^{3d}} e^{\mathrm{i}\kappa\widehat{x}\cdot x}\left(\frac{1}{R_\Omega}+\mathrm{i}\kappa+\mathrm{i}\kappa\widehat{x}\cdot n\right)\delta p_h. \tag{37}$$

Here δp_h denotes the variation of p_h due to the variation $\delta\alpha_h$. Note that, in expression (37), the variation affects only p_h since Γ_{out} and all other terms do not depend on α_h.

The relation between $\delta\alpha_h$ and $\delta p_{h,\infty}$ can be established from linearization of the state equation (15). By differentiating the discrete state equation (15) with respect to the variation $\delta\alpha_h$, we get

$$\begin{aligned}
&\int_{\Omega_0} r\nabla\delta p_h\cdot\nabla q_h - \kappa^2\int_{\Omega_0} r\delta p_h q_h + \mathrm{i}\kappa\int_{\Gamma_{\text{in}}\cup\Gamma_{\text{out}}} r\delta p_h q_h + \int_{\Gamma_{\text{I}}} r\lambda[\![\delta p_h]\!][\![q_h]\!] + \int_{\Gamma_{\text{I}}} r\delta\lambda[\![p_h]\!][\![q_h]\!] \\
&\quad - \int_{\Gamma_{\text{I}}} rc_1\Big([\![q_h]\!]\left\{\frac{\partial\delta p_h}{\partial n}\right\} + [\![\delta p_h]\!]\left\{\frac{\partial q_h}{\partial n}\right\}\Big) - \int_{\Gamma_{\text{I}}} rc_2\left\{\frac{\partial\delta p_h}{\partial n}\right\}\left\{\frac{\partial q_h}{\partial n}\right\} \\
&\quad - \int_{\Gamma_{\text{I}}} r\delta c_1\Big([\![q_h]\!]\left\{\frac{\partial p_h}{\partial n}\right\} + [\![p_h]\!]\left\{\frac{\partial q_h}{\partial n}\right\}\Big) - \int_{\Gamma_{\text{I}}} r\delta c_2\left\{\frac{\partial p_h}{\partial n}\right\}\left\{\frac{\partial q_h}{\partial n}\right\} = 0,
\end{aligned} \tag{38}$$

for all $q_h \in V_h$. Equation (38) can be rewritten as

$$\begin{aligned}
a_\lambda(\alpha_h;\delta p_h, q_h) &- \int_{\Gamma_{\text{I}}} \delta c_1\Big([\![q_h]\!]\left\{\frac{\partial p_h}{\partial n}\right\} + [\![p_h]\!]\left\{\frac{\partial q_h}{\partial n}\right\}\Big) \\
&- \int_{\Gamma_{\text{I}}} \delta c_2\left\{\frac{\partial p_h}{\partial n}\right\}\left\{\frac{\partial q_h}{\partial n}\right\} + \int_{\Gamma_{\text{I}}} \delta\lambda[\![p_h]\!][\![q_h]\!] = 0.
\end{aligned} \tag{39}$$

Let z_h be the solution to the following adjoint problem

$$\begin{aligned}
&\text{Find } z_h \in V_h \text{ such that} \\
&\quad a_\lambda(\alpha_h; v_h, z_h) = v_{h,\infty}(\theta) \ \ \forall v_h \in V_h,
\end{aligned} \tag{40}$$

where

$$v_{h,\infty}(\theta) = \frac{1}{4\pi}\int_{\Gamma^{3d}_{\text{out}}} e^{\mathrm{i}\kappa\widehat{x}\cdot x}\left(\frac{1}{R_\Omega} + \mathrm{i}\kappa + \mathrm{i}\kappa\widehat{x}\cdot n\right) v_h. \tag{41}$$

In equations (38) and (39), $q_h \in V_h$ is arbitrary. By choosing $q_h = z_h$ in equation (39) where z_h is the solution adjoint problem (40), we obtain

$$\begin{aligned}
a_\lambda(\alpha_h;\delta p_h, z_h) &- \int_{\Gamma_{\text{I}}} r\delta c_1\Big([\![z_h]\!]\left\{\frac{\partial p_h}{\partial n}\right\} + [\![p_h]\!]\left\{\frac{\partial z_h}{\partial n}\right\}\Big) \\
&- \int_{\Gamma_{\text{I}}} r\delta c_2\left\{\frac{\partial p_h}{\partial n}\right\}\left\{\frac{\partial z_h}{\partial n}\right\} + \int_{\Gamma_{\text{I}}} r\delta\lambda[\![p_h]\!][\![z_h]\!] = 0.
\end{aligned} \tag{42}$$

Similarly, by choosing $v_h = \delta p_h$ in the adjoint equation (40), we get

$$a_\lambda(\alpha_h;\delta p_h, z_h) = \delta p_{h,\infty}(\theta), \tag{43}$$

where $\delta p_{h,\infty}(\theta)$ is as defined in expression (37). By combining expressions (42) and (43), we find

$$\begin{aligned}\delta p_{h,\infty}(\theta) = &\int_{\Gamma_{\rm I}} r\delta c_1 \Big([\![z_h]\!] \left\{ \frac{\partial p_h}{\partial n} \right\} + [\![p_h]\!] \left\{ \frac{\partial z_h}{\partial n} \right\} \Big) \\ &+ \int_{\Gamma_{\rm I}} r\delta c_2 \left\{ \frac{\partial p_h}{\partial n} \right\} \left\{ \frac{\partial z_h}{\partial n} \right\} - \int_{\Gamma_{\rm I}} r\delta\lambda [\![p_h]\!] [\![z_h]\!] = 0.\end{aligned} \tag{44}$$

The variations of c_1, c_2, and λ in expression (44), using the product and chain rules, are

$$\begin{aligned}\delta\lambda &= -\frac{1}{\mathrm{i}\kappa}\lambda^2\,\delta\zeta_h, \\ \delta c_1 &= -\frac{1}{\mathrm{i}\kappa}\Big(\lambda\,\delta\zeta_h + \zeta_h\,\delta\lambda\Big) = -\frac{1}{\mathrm{i}\kappa}\Big(\lambda - \frac{1}{\mathrm{i}\kappa}\lambda^2\zeta_h\Big)\,\delta\zeta_h, \\ \delta c_2 &= \frac{1}{\mathrm{i}\kappa}\left(\delta\zeta_h - \frac{\zeta_h}{\mathrm{i}\kappa}\Big(2\lambda\,\delta\zeta_h + \zeta_h\,\delta\lambda\Big)\right) = \frac{1}{\mathrm{i}\kappa}\left(1 - \frac{\zeta_h}{\mathrm{i}\kappa}\Big(2\lambda - \frac{1}{\mathrm{i}\kappa}\lambda^2\zeta_h\Big)\right)\,\delta\zeta_h.\end{aligned} \tag{45}$$

Thus, by using the variation of ζ_h with respect to $\delta\alpha_h$, expressions (44) and (45) establish the required relation between $\delta\alpha_h$ and $\delta p_{h,\infty}$ in terms of the solution of the adjoint equation (40). By using the relation between the differential and the partial derivative $\delta h = \delta a_i \partial h/\partial a_i$ and noting that a_i is the value of α_h in element E_i, from expression (45) we find that

$$\begin{aligned}\frac{d\lambda}{da_i} &= -\frac{1}{\mathrm{i}\kappa}\lambda_i^2\frac{d\zeta_{h,i}}{da_i}, \\ \frac{dc_1}{da_i} &= -\frac{1}{\mathrm{i}\kappa}\Big(\lambda_i - \frac{1}{\mathrm{i}\kappa}\lambda_i^2\zeta_{h,i}\Big)\frac{d\zeta_{h,i}}{da_i}, \\ \frac{dc_2}{da_i} &= \frac{1}{\mathrm{i}\kappa}\left(1 - \frac{\zeta_{h,i}}{\mathrm{i}\kappa}\Big(2\lambda_i - \frac{1}{\mathrm{i}\kappa}\lambda_i^2\zeta_{h,i}\Big)\right)\frac{d\zeta_{h,i}}{da_i},\end{aligned} \tag{46}$$

where $\lambda_i = \lambda|_{E_i}$ and $\zeta_{h,i} = \zeta_h(a_i)$. Note the derivative $d\zeta_{h,i}/da_i$ depends on the parametrization of $\zeta_{h,i}$; see discussion in §9 below. The gradients of g_1 and g_2 with respect to a_i, (note that a_i is real), are given by

$$\begin{aligned}\frac{\partial g_1}{\partial a_i} &= \mathfrak{R}(\partial p_{h,\infty}/\partial a_i), \\ \frac{\partial g_2}{\partial a_i} &= \mathfrak{I}(\partial p_{h,\infty}/\partial a_i),\end{aligned} \tag{47}$$

respectively, where

$$\begin{aligned}\frac{\partial p_{h,\infty}(\theta)}{\partial a_i} = &\int_{E_i} \frac{dc_1}{da_i} r \left([\![z_h]\!] \left\{ \frac{\partial p_h}{\partial n} \right\} + [\![p_h]\!] \left\{ \frac{\partial z_h}{\partial n} \right\} \right) + \int_{E_i} \frac{dc_2}{da_i} r \left\{ \frac{\partial z_h}{\partial n} \right\} \left\{ \frac{\partial p_h}{\partial n} \right\} \\ &- \int_{E_i} \frac{d\lambda}{da_i} r [\![z_h]\!] [\![p_h]\!].\end{aligned} \tag{48}$$

The derivative of I_h with respect to a_i is

$$\frac{\partial I_h(\theta)}{\partial a_i} = 2g_1 \frac{\partial g_1}{\partial a_i} + 2g_2 \frac{\partial g_2}{\partial a_i}. \tag{49}$$

Now, rewrite the objective function (20) as

$$J_h(\mathbf{a}; f, \theta_1, \theta_2) = \frac{1}{2} \log_{10}\big(I_h(\theta_1)\big) - \frac{1}{2} \log_{10}\big(I_h(\theta_2)\big). \tag{50}$$

Then, the derivative of $J_h(\mathbf{a}, f, \theta_1, \theta_2)$ with respect to a_i, using the chain rule and expressions (47) and (49), is given by

$$\frac{\partial J_h(\mathbf{a}; f, \theta_1, \theta_2)}{\partial a_i} = \frac{1}{2\ln(10)} \left(\frac{1}{I_h(\theta_1)} \frac{\partial I_h(\theta_1)}{\partial a_i} - \frac{1}{I_h(\theta_2)} \frac{\partial I_h(\theta_2)}{\partial a_i} \right). \tag{51}$$

Alternatively, we can rewrite in the following form, by expressions (34), (47), and (49),

$$\frac{\partial J_h(\mathbf{a}; f, \theta_1, \theta_2)}{\partial a_i} = \frac{G(\theta_1) - G(\theta_2)}{\ln(10)}, \tag{52}$$

where

$$G(\theta) = \frac{1}{|p_{h,\infty}(\theta)|^2} \left(\Re\{p_{h,\infty}(\theta)\} \Re\left\{ \frac{\partial p_{h,\infty}(\theta)}{\partial a_i} \right\} + \Im\{p_{h,\infty}(\theta)\} \Im\left\{ \frac{\partial p_{h,\infty}(\theta)}{\partial a_i} \right\} \right), \tag{53}$$

in which $\partial p_{h,\infty}(\theta)/\partial a_i$ is given by expression (48).

Note that since the bilinear form a_λ is symmetric, adjoint problem (40) and variational problem (15) have the same system matrix. Thus, the same system matrix factorization can thus be used to solve both systems, which will save computational time. The forward and adjoint systems are also uncoupled and can be solved in parallel.

9 Numerical Verification

In this section, we verify the gradient computation against a finite difference approximation. We compute the derivatives of objective function (20) using formula (52) and compare the values obtained by a first-order finite difference approximation. The derivative of the objective function with respect to design variable a_i can be approximated using a forward finite difference

$$\frac{\partial J_h(\mathbf{a}; f, \theta_1, \theta_2)}{\partial a_i} \approx \frac{J_h(\mathbf{a} + \delta \mathbf{e}_i; f, \theta_1, \theta_2) - J_h(\mathbf{a}; f, \theta_1, \theta_2)}{\delta} \tag{54}$$

where $\mathbf{e}_i$ is the i^{th} column of an identity matrix of size equal to the number of design variables and δ is a step size.

Table 1: *The dimensions of the horn in terms of the parameters are as defined in Figures 1 and 2*

a (mm)	b (mm)	l (mm)	d (mm)	R_Ω (mm)
19.3	150	161.5	206.5	400

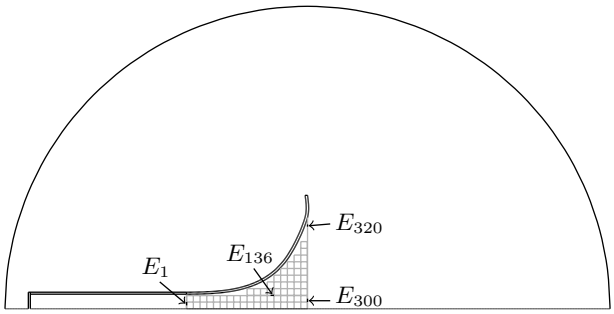

Figure 6: The position of the design variables where the derivatives are computed.

We consider a cylindrical horn in Figure 1 with with dimensions as given in Table 1. The shape of the horn was determined by gradient-based shape optimization [14]. We partition the horn region Ω_{H}, illustrated in Figure 2, into 68 subdomains by putting 67 squares with side length 8.9722 mm as depicted in Figure 4. The partitioning introduces an interface Γ_{I} consisting of 146 components. The components are boundaries between the subdomains. The finite element discretization in subdomain $\Omega_i,\ i = 1, \ldots, 70$, including Ω_{W} and Ω_{A}, uses second order triangular elements on an unstructured mesh. The mesh with maximum element size of $h = 4.4861$ mm is generated by Comsol Multiphysics. The incoming plane wave traveling into the waveguide has an amplitude of $A = 1$ at the inlet boundary Γ_{in} and a frequency of 5702 Hz.

When the derivatives are computed, we assume that design variable a_i, the value of α_h on interface boundary E_i, have the same value for all i. The derivative $\partial J_h/\partial a_i$ is considered at four interface boundary elements, E_i, for $i = 1, 136, 300$, and 320. The positions of the elements on the grid line are depicted in Figure 6. We compute the gradient for five different values of the design variable in the range between 0 and 1.

We assume impedance function ζ_h is purely imaginary. In this case there is no acoustic loss on the interface Γ_{I}. We consider two impedance parametrizations and we use $\delta = 1e^{-7}$ as a step size for all finite difference calculations. Table 2 shows the derivatives when the impedance is a cubic function of the the design variable, that is, $\zeta_h = 50\mathrm{i}(1-\alpha_h)^3$. The derivatives in Table 3 is when $\zeta_h = 50\mathrm{i}(1-\alpha_h)$. In this case, the derivatives with respect to the impedance can be determined from $\partial J_h/\partial a_i$ by scaling. The tables shows derivatives computed by the adjoint method (denoted by AM) and the finite difference method (denoted by FD). The absolute difference

Table 2: *Derivatives of the objective function with respect to the design variables located at* E_i, $i = 1, 136, 300, 320$ *(Figure 3). The derivatives are computed by using adjoint method (AM) and finite difference (FD) for* $\zeta_h = 50i(1-\alpha_h)^3$. $|AD-FD|$ *denotes the absolute difference between the gradients computed by AM and FM.*

a	J_h	$\partial J_h/\partial a_i$	$\partial J_h/\partial a_1$	$\partial J_h/\partial a_{136}$	$\partial J_h/\partial a_{300}$	$\partial J_h/\partial a_{320}$
		AM	2.2126e-15	5.7815e-15	3.4746e-03	1.3647e-02
0	1.7374	FD	2.4424e-12	5.5511e-12	3.4746e-03	1.3647e-02
		|AD−FD|	2.4402e-12	5.5453e-12	2.5382e-09	3.2531e-08
		AM	1.4223e-15	5.0961e-11	1.1581e-02	-2.0798e-04
0.25	1.7589	FD	3.5527e-12	7.2830e-11	1.1581e-02	-2.0798e-04
		|AD−FD|	3.5512e-12	2.1868e-11	1.2882e-09	3.0585e-10
		AM	1.4921e-02	4.2879e-01	-2.0862e-00	-1.9575e-03
0.5	1.6996	FD	1.4921e-02	4.2879e-01	-2.0862e-00	-1.9575e-03
		|AD−FD|	1.3982e-07	4.2560e-08	2.7748e-07	1.0092e-09
		AM	1.5913e-03	3.6825e-02	-1.4516e-01	-2.5055e-02
0.75	1.7782	FD	1.5913e-03	3.6825e-02	-1.4516e-01	-2.5055e-02
		|AD−FD|	3.6856e-09	9.4940e-08	2.9388e-07	2.5312e-08
		AM	0	0	0	0
1	1.5712	FD	3.3306e-12	-9.7699e-10	-3.7747e-09	-2.4202e-09
		|AD−FD|	3.3306e-12	9.7699e-10	3.7747e-09	2.4202e-09

between the gradients computed by the adjoint and finite difference methods is denoted by |AD−FD|. From Tables 2 and 3, we note that the derivatives depend on the position and the value of the design variable. In general, from Tables 2 and 3, we can see that the objective function is more sensitive for the variations in the design variable around the mouth of the horn. For derivatives note close to zero, the derivatives computed by the adjoint method and the finite difference approximations agree up to 6 significant digits for both impedance parameterizations.

Table 3: *Derivatives of the objective function with respect to the design variables located at* E_i, $i = 1, 136, 300, 320$ *(Figure 3). The derivatives are computed by using adjoint method (AM) and finite difference (FD) for* $\zeta_h = 50i(1 - \alpha_h)$. $|AD-FD|$ *denotes the absolute difference between the gradients computed by AM and FM.*

a	J_h	$\partial J_h/\partial a_i$	$\partial J_h/\partial a_1$	$\partial J_h/\partial a_{136}$	$\partial J_h/\partial a_{300}$	$\partial J_h/\partial a_{320}$
		AM	7.3793e-16	1.9271e-15	1.1582e-03	4.5492e-03
0	1.7374	FD	5.1070e-12	1.3322e-12	1.1582e-03	4.5492e-03
		$\lvert$AD$-$FD$\rvert$	5.1062e-12	1.3303e-12	4.7050e-09	1.4439e-09
		AM	3.8121e-16	2.7406e-14	2.1638e-03	4.0303e-03
0.25	1.7452	FD	8.8817e-12	1.5987e-11	2.1638e-03	4.0303e-03
		$\lvert$AD$-$FD$\rvert$	8.8814e-12	1.5959e-11	2.6269e-09	2.8593e-09
		AM	1.6423e-16	1.9470e-12	4.9880e-03	1.5060e-03
0.5	1.7555	FD	3.1086e-12	4.8849e-12	4.9880e-03	1.5060e-03
		$\lvert$AD$-$FD$\rvert$	3.1084e-12	2.9379e-12	3.7239e-09	8.1430e-09
		AM	-8.4619e-15	4.3012e-08	1.4559e-02	-2.5243e-03
0.75	1.7645	FD	-4.4408e-12	4.2859e-08	1.4559e-02	-2.5243e-03
		$\lvert$AD$-$FD$\rvert$	4.4324e-12	2.2316e-10	8.6554e-08	6.5137e-09
		AM	5.1375e-06	-6.2218e-01	-5.9230e-01	-1.1288e-02
1	1.5712	FD	5.1070e-06	-6.2218e-01	-5.9230e-01	-1.1287e-02
		$\lvert$AD$-$FD$\rvert$	3.0551e-09	1.8694e-07	2.5523e-07	1.0686e-08

Acknowledgements

I am grateful to Martin Berggren and Eddie Wadbro for many fruitful discussions and carefully reading the manuscript and giving constructive comments. This research was supported in part by the Swedish Foundation for Strategic Research, Grant No. AM13-0029, and by the Swedish Research Council, Grant No. 621-2013-3706.

References

[1] M. P. Bendsøe and O. Sigmund. *Topology optimization. Theory, methods, and applications*. Springer, 2003.

[2] E. L. Yedeg, E. Wadbro, and M. Berggren. Interior layout topology optimization of a reactive muffler. *Struct. Multidiscip. Opt.*, 53:634–656, 2016. Doi: 10.1007/s00158-015-1317-x.

[3] Eddie Wadbro, Rajitha Udawalpola, and Martin Berggren. Shape and topology optimization of an acoustic horn–lens combination. *J. Comput. Appl. Math.*, 234(6):1781–1787, 2010. Doi: 10.1016/j.cam.2009.08.028.

[4] Seong-Hyun Lee and Jeong-Guon Ih. Empirical model of the acoustic impedance of a circular orifice in grazing mean flow. *jasa*, 114(1):98–113, 2003. DOI: 10.1121/1.1581280.

[5] S. W. Rienstra and A. Hirschberg. An introduction to acoustics. Revised and updated version of reports IWDE 92-06 and IWDE 01-03, Eindhoven University of Technology, 2015.

[6] E. L. Yedeg, E. Wadbro, P. Hansbo, M. G. Larson, and M. Berggren. A Nitsche-type method for Helmholtz equation with an embedded acoustically permeable interface. *Comput. Methods Appl. Mech. Engrg.*, 304:479–500, 2016. Doi:10.1016/j.cma.2016.02.032.

[7] P. W. Christensen and A. Klarbring. *An Introduction to Structural Optimization*, volume 153 of *Solid Mechanics and Its Applications*. Springer, 2008.

[8] B. Engquist and A. Majda. Absorbing boundary conditions for the numerical simulation of waves. *Mathematics of Computation*, 31(139):629 –651, 1977.

[9] F. Ihlenburg. *Finite Element Analysis of Acoustic Scattering*. Springer, New York, 1998.

[10] Eddie. Wadbro. On the far-field properties of an acoustic horn. *Technical report 2006-042, Department of Information Technology, Uppsala University*, 2006.

[11] D. Colton and R. Kress. *Integral Equation Methods in Scattering Theory*. Classics in Applied Mathematics. Society for Industrial and Applied Mathematics, 2013.

[12] J. Nitsche. Über ein Variationsprinzip zur Lösung von Dirichlet-Problemen bei Verwendung von Teilräumen, die keinen Randbedingungen unterworfen sind. *Abh. Math. Sem. Univ. Hamburg*, 36:9–15, 1971. Doi: 10.1007/BF02995904.

[13] Rajitha Udawalpola and Martin Berggren. Optimization of an acoustic horn with respect to efficiency and directivity. *International Journal for Numerical Methods in Engineering*, 73(11):1571–1606, 2008. Doi:10.1002/nme.2132.

[14] Daniel Noreland, Rajitha Udawalpola, Pablo Seoane, Eddie Wadbro, and Martin Berggren. An efficient loudspeaker horn designed by numerical optimization: An experimental study. *Report UMINF 10.1, Department of Computing Science, Umeå University*, 2010.